

Accounting SDR Fluctuations to Non-Premixed Turbulent Combustion for Better Predictions of In-Cylinder Processes

Dr. S.M.Jameel Basha

¹Principal, VIF College Of Engineering and Technology, Hyderabad.

ABSTRACT

The In-cylinder gas flow is complex three dimensional, unsteady and turbulent and hence poses many problems and uncertainties in the theoretical predictions. Of course, to study and have a better understanding of such combustion processes, the simulation models are more suitable compared to the time consuming experimental methods. The computational Fluid Dynamic models have gained momentum with the advent of high end computers for analysis of IC engine combustion process.

FLUENT is the versatile tool for modeling the dynamic mesh parameters, in-cylinder flows and better analysis of pollutants. It is found that ignoring the effect of Scalar Dissipation Rate Fluctuations may cause inconsistency in predictions. Hence it is aimed to adopt Scalar Dissipation Rate Fluctuations by writing the User Defined Function (UDF) and appending it to existing code.

Air motion which depends on piston bowl configuration plays important role in fuel-air mixing, combustion and emission formation especially at the end of compression stroke at TDC. In order to understand this effect, spherical bowl configuration was chosen for computations. The predicted results were compared with and without piston bowl configuration to include scalar dissipation rate fluctuations (SDRF). The validation of the modified computer code is done by comparing the measured available data. Results were presented in the form of temperature, pressure and TKE contours gives better analysis of in-cylinder processes.

Keywords: SDRF, CFD, Flamelet equation, PDF

I. INTRODUCTION

The process of combustion in diesel engines generally takes place at heterogeneous fuel vapor-air mixture. The theory of combustion is very complex and lots of researchers were attracted towards it. The rate of combustion is determined by the velocity of mutual diffusion of fuel vapors and air and the rate of chemical reaction is of minor importance. It is unsteady, heterogeneous and three dimensional process.

II. PROBLEM DEFINITION

The modeling of engine processes continues to develop as our basic understanding of the physics and chemistry of the phenomena of interest steadily expands as the capability of computers to solve complex equations continues to increase. The modeling results are inconsistent when compared with the experimental results and the reasons are attributed to lot of restrictions and assumptions used in modeling methods. In the present work it is observed that one effect scalar dissipation rate fluctuations henceforth called as SDRF is neglected and possible inclusion of SDRF is analyzed. Fluid dynamic code FLUENT is selected in the present work because the code has greater flexibility suitable to different applications.

III. THEORY OF COMPUTATION

In technical process, combustion always takes place within a turbulent rather than a laminar flow field. The reason for this is twofold: First, turbulence increases the mixing processes and thereby enhances combustion. Second, combustion releases heat and thereby generates flow instability by buoyancy and gas expansion, which then enhances the transition to turbulence.[1]

The turbulence combustion models rely on the modeling procedures which are highly disputed because they rely on empiricism and some kind of intuition supplemented by physical arguments [2]. It is clear that with combustion, empiricism and the number of necessary simplifications increase. This is reflected by the large variety of different combustion models that have been formulated and that are pursued and continuously improved by different groups in the combustion community.

Combustion essentially takes place in the vicinity of the surface of stoichiometric mixture. The temperature equation is

$$\rho \left(\frac{\partial T}{\partial t} + \sum_{k=2}^3 v_k \frac{\partial T}{\partial x_k} \right) = \rho \frac{x}{2} \frac{\partial^2 T}{\partial Z^2} + \sum_{k=2}^3 \frac{\partial}{\partial x_k} \left(\rho D \frac{\partial T}{\partial x_k} \right) + \frac{1}{cp} \frac{\partial P}{\partial t} - \frac{1}{cp} \sum_{i=1}^N h_i m_i + 2\rho D \sum_{k=2}^3 \frac{\partial Z}{\partial x_k} \frac{\partial^2 T}{\partial Z \partial x_k} - \frac{1}{cp} \frac{\partial f_k}{\partial x_k}$$

.....1

$$X = 2D \left(\frac{\partial Z}{\partial x_k} \right)^2 \dots\dots\dots 2$$

If the flamelet is thin in the Z direction an order of magnitude analysis similar to that for a boundary layer shows that the second derivative with respect to Z is a dominating term on the R.H.S of equation 1. To lead the order in an asymptotic analysis this term must balance the reaction term on the right hand side. The term containing the time derivative is only important if very rapid changes such as extinction, occurs. If the time derivative term is retained, the flamelet structure is to leading order described by the one dimensional time dependent temperature equation.

$$\rho \frac{\partial T}{\partial t} = \rho \frac{X}{2} \frac{\partial^2 T}{\partial Z^2} - \frac{1}{cp} \sum_{i=1}^N h_i m_i + \frac{1}{cp} \frac{\partial P}{\partial t} - \frac{1}{cp} \frac{\partial T_k}{\partial X_k} \dots\dots\dots 3$$

$$\rho \frac{\partial y_i}{\partial t} = \frac{1}{2} \rho \frac{\partial^2 y_i}{\partial Z^2} + \omega_i \dots\dots\dots 4$$

Effects of turbulent flow are parameterized and imposed in the flamelet by the instantaneous scalar dissipation rate. It has the dimension sec⁻¹ and may be interpreted as the inverse of characteristic diffusion time. Due to the transformation it implicitly incorporates the influence of convection and diffusion normal to the surface of stoichiometric mixture. In the limit of X=0.0 the chemical source term (ω_i) must sum to zero if transient and radiation loss terms are neglected.

For the counter flow geometry, the scalar dissipation rate at the location where the mixture is stoichiometric may be approximated assuming constant density and diffusivity by

$$X_{st} = 4a Z_{st}^2 [\text{erfc}^{-1}(2Z_{st})]^2 \dots\dots\dots 5$$

Where 'a' is the velocity gradient and erfc⁻¹ the inverse of complementary error function.

Equation 3 has been written with a scalar dissipation that varies with Z and possibly time. It also contains the unsteady term. First order terms in equation 3 that have been neglected are the convection term and the last but one term on the R.H.S which represents curvature effects. The second term on the R.H.S describes diffusion along lines of constant mixture fraction and comes in at second order only.

The scalar dissipation rate can be expanded around Z_{st} as

$$X = X_{st} + \left(\frac{\partial X}{\partial Z} \right)_{Z_{st}} (Z - Z_{st}) \dots\dots\dots 6$$

Since Z-Z_{st} is small in the reaction zone this expansion introduces a first order term with an

additional parameter. $\left(\frac{\partial X}{\partial Z} \right)_{st}$. This term is not small

and its fluctuations in a turbulent flow should be considered. Unsteady effects have been analyzed by in a lagrangian simulation of flamelet extinction by solving the unsteady flamelet equations with a spatially constant but time- varying value of X_{st}.

3.1 Random scalar dissipation fluctuations in non-premixed combustion:

The basic purpose is to analyze how random fluctuations of the scalar dissipation rate can affect extinction of non-premixed combustible systems. The approach based on stochastic differential equations, allows taking random extinction events into account. The probability density function for the temperature in the reaction will undergo fluctuations increases. In the present work, the non dimensional flamelet equations for a one-step global reaction with this assumption the system can be reduced to a single equation for the temperature. Stochastic differential equations for the temperature and the scalar dissipation rate were derived and discussed and numerical solutions are presented here.

3.2 Flamelet equations

Assuming an irreversible one-step reaction of the form $\nu_F F + \nu_O D \rightarrow P \nu$

Where F,O and D denote the fuel, oxidizer and reaction product respectively, the flamelet equations for the mass fractions of fuel y_F, oxidizer y_O reaction product y_P and temperature T

$$\frac{\partial y_i}{\partial t} - \frac{x}{2} \frac{\partial^2 y_i}{\partial Z^2} + \nu_i W_i \omega = 0.0 \dots\dots\dots 7$$

i = F,O,P

$$\frac{\partial T}{\partial t} - \frac{x}{2} \frac{\partial^2 T}{\partial Z^2} - \frac{Q}{cp} \omega = 0.0 \dots\dots\dots 8$$

$$\text{Where } Q = - \sum_{i=1}^N \nu_i W_i h_i \dots\dots\dots 9$$

By non dimensionalization the temperature θ and mass fraction of fuel, oxidizer and reaction product a joint PDF of the temperature and scalar dissipation rate is derived. By considering strantonovich differential equation that governs the evolution of the scalar dissipation rate,

$$\omega = \frac{D_a (1 - \alpha) \exp(\beta_{ref} - \beta)}{1 - \alpha(1 - \theta_{st})} (1 - \theta_{st})^2 \exp\left(- \frac{Z_e (1 - \theta_{st})}{1 - \alpha(1 - \theta_{st})} \right) \dots\dots\dots 10$$

This equation gives random fluctuations of the scalar dissipation rate on non premixed combustion process.

The tangential velocity vectors at selected planes within the piston bowl are presented which depict the true information of the flow field.

IV. RESULTS AND DISCUSSION

The results obtained with and without SDRF inclusion are compared. Also the results are validated with the available experimental data and good agreement is noticed. The consistency and reduction in the error percentage in results are observed by taking into account the scalar dissipation rate fluctuations.

4.1 Modeling, Meshing and post processing of results: Model is created using GAMBIT.

For Hemispherical bowl the meshing is done using hexahedral elements. The number of cells considered for meshing is around 654400.

FLUENT 6.3 Version [5] is used for solving and for post processing the results.

4.2 Presentation of results:

The results pertaining to test computations for an engine fitted with a hemispherical bowl-in-piston is discussed.

4.3 Test Computations:

These computations pertain to the test engine fitted with hemi-spherical bowl-in-piston. Fig 4.1 shows the view of typical mesh which represents the in-cylinder flow field. The computed pressure histories considering the effect of SDRF and ignoring SDRF is compared with the available measured pressure histories.

4.3.1 Comparison of experimental and predicted pressure histories:

Figure 4.2 gives the comparison of the predicted and experimental pressure histories. A good agreement is obtained during compression. The predicted pressures are slightly higher during the combustion and the small deviation between the two goes hand in hand during the later part of expansion stroke. In the normal engine operation, the in-cylinder charge prior to the combustion contains some portion of residual gases which could not be exhausted completely in the previous cycle. But only pure air without any residual gas is assumed to be compressed, in the present modeling. Hence higher predicted combustion pressures are resulted. The predicted peak pressures without SDRF, experimental [6] and with SDRF are 7.147 MPa, 6.829 MPa and 7.01Mpa respectively. The %error in the predicted peak pressure without SDRF and experimental value is 4.449% and the %error in the

predicted peak pressure with SDRF and experimental value is 2.58%.

4.3.2 Variation of temperature with crank angle:

Temperature inside the engine cylinder is almost the lowest at the end of the suction stroke. During combustion, there is a rapid rise in temperature to a peak value which again drops during the expansion. Fig 4.3 gives the comparison between predicted without SDRF, experimental and predicted with SDRF values for cylinder temperatures. The maximum cylinder temperature attained is 2620.61 k, 2601.9 k and 2610 for without SDRF, experimental and with SDRF values respectively. The problem with the attainment of high temperatures in the engine cylinder is that the high temperatures are responsible for the formation of NO_x at high temperature.

4.3.3 Variation of total energy with crank angle:

Figure 4.4 shows the variation of total energy with crank angle. The peak energy reached during the operating cycle is 449 KJ/kg without SDRF, 429 KJ/kg for experimental and 442 KJ/kg for with SDRF. Generally it is more difficult to determine the start of combustion precisely. It is normally identified from the change in slope of the heat release rate. The pressure rate alone may indicate this, when the pressure change first occurs due to combustion. The cumulative energy only increases when there is start of combustion and prior to that no substantial growth in energy is noticed.

4.4 Temperature contours:

As a part of the result, the temperature contour plots are presented which give the information about the local temperature distributions in the combustion chamber domain. The predictions of the temperature distribution will assist the designer to avoid local hot spots which may cause pre-ignition of the charge and severe local thermal stresses [7].

The heat flux and heat transfer between locations in the combustion chamber will be non uniform. The local temperature zones in the combustion chamber are difficult to estimate since the in-cylinder heat transfer is unsteady. But, to know the local temperature zones and get an idea about the local hot spots which cause pre-ignition, the temperature contour plots are pointed for the local temperature development from the simulation and respective distributions for different crank angles is shown in the fig 4.5.

The temperature, pressure, TKE contours along with in-cylinder flow predictions such as velocity vectors are presented by selecting the surfaces called as surface-0. The post processing results can be

presented by selecting other surfaces also but it is convenient to present the results at this surface.

At crank angle 28 degrees bTDC [fig 4.5 (a₁)], the temperature at the bowl centre is about 2230 k indicating the initiation of combustion whereas the rest of the combustion chamber remains at the temperature of 626 k, fig 4.5 (a₂) gives the variation considering the effect of SDRF at the same crank angle. The effect of SDRF is very high after start of injection but strongly decreases with time due to turbulent mixing process. Fig 4.10 (b₁ and b₂) illustrates the variation in the local temperatures due to commencement of injection. Fig 4.5 (b₂) shows the effect of SDRF, which elucidates the reduction in cylinder temperature. The injection was done from four nozzles injecting 2000 particles per injector. Due to non symmetric injection, the particles were unable to penetrate to one corner of the cylinder due to evaporation of the droplet.

The variation of these local temperatures is drastically increased as soon as the combustion commences. Fig 4.5 (c₁) to (d₁) illustrates this without SDRF and fig 4.5 (c₂) to (d₂) shows the effect of SDRF. Fig 4.5 (e₁) shows when crank angle is 5⁰ bTDC represents the maximum cycle temperature of 2950 k. Fig 4.5(e₂) shows when crank angle is 5⁰ bTDC considering the effect of SDRF. The maximum cycle temperature with SDRF is 2630 k. As the piston moves away from the TDC, there will be downtrend observed in temperatures. Temperature gradually reduces due to the expansion of the gases in the cylinder, which can be observed from the figures 4.5 (e₁ and e₂) and 4.5 (f₁ and f₂).

4.5. Pressure contours:

The pressure contours are presented in figure 4.6. Figures for different crank angles of the piston movement from 28⁰ bTDC, 10⁰ bTDC, 5⁰ TDC, TDC, 5⁰ aTDC and 10⁰ aTDC are presented. At the crank angle 28⁰ bTDC [Fig 4.6 (a₁)] the predicted pressure is 1.32 MPa and it raises upto 7.15 MPa when the crank angle is at 5⁰ aTDC [Fig 4.6 (e₁)] which is the maximum cycle pressure. The pressure which is built inside the combustion chamber gradually reduces when the piston moves towards BDC. The same is illustrated in the figure 4.6 (f₁). Fig 4.6(a₂, b₂, c₂, d₂, e₂ and f₂) show the effect on

pressure contours considering SDRF. The maximum cycle pressure considering SDRF is 7.0 MPa compared to predicted maximum cycle pressure of 7.15 MPa. This is attributed to the fact that unsteady fluctuations of the scalar dissipation are likely to suppress the ignition, consequently, the pressure and the temperature of the cycle. The tremendous raise in pressure from 28⁰ bTDC upto TDC represents the reduced delay period and normal combustion. The pressure parameter has very great influence on the performance of the engine.

4.6 Turbulent kinetic energy contours:

The contour plots for turbulent kinetic energy are useful to locate the zones of turbulent flows. It is possible to know the variation of intensity of turbulence in the engine combustion chamber from these diagrams. The turbulent kinetic energy is found to increase with the radius reaching to a maximum near the cylinder wall [8]. After the start of fuel injection, turbulent kinetic energy contours exhibit a different tendency.

At crank angle 28⁰ bTDC [fig 4.7 (a₁)] it is noticed, that turbulent kinetic energy at the injector tip is several times higher than the surrounding region.

At crank position 10⁰bTDC [fig 4.7 (b₁)] the maximum TKE is noticed on the surface of the bowl region near to neck. At 5⁰ bTDC [4.7 (c₁)] the peak TKE of the cycle is noticed. This sudden variation is due to rapid progress in combustion in the combustion chamber. The values of local TKE at further crank angle intervals are found decreasing, [fig 4.7 (d₁), (e₁) and (f₁)]. Fig 4.7 (a₂, b₂, c₂, d₂, e₂ and f₂) shows the variation of TKE considering the effect of SDRF. The TKE is suppressed due to the effect of SDRF when compared with the predicted TKE values without SDRF because the air particles cannot propagate in or around the clouds of droplets and it is possible to observe some local extinction. The variation of TKE increases during compression stroke and found almost dropping their values during the expansion stroke.

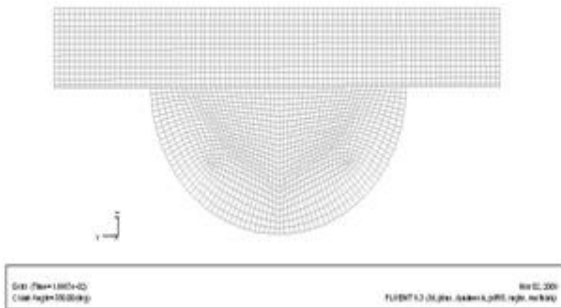


Fig 4.1 Computational mesh of hemispherical bowl

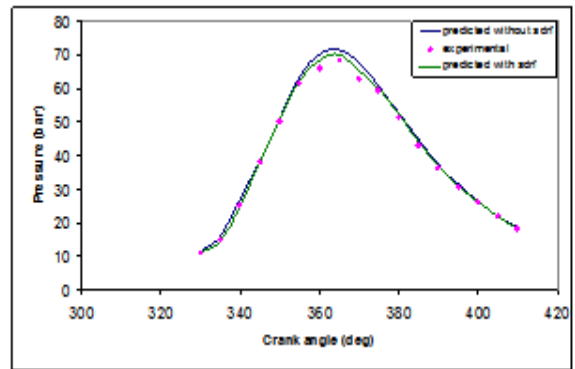


Fig 4.2 Variation of cylinder pressure with crank angle

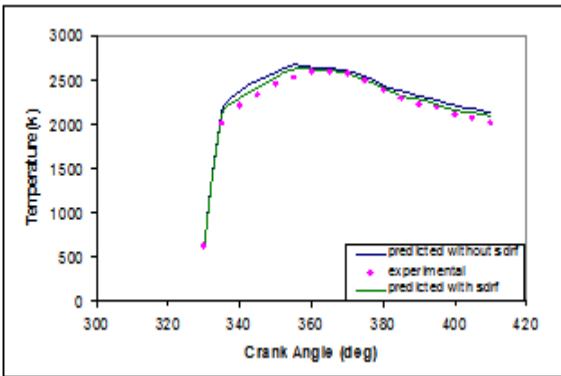


Fig 4.3 Variation of temperature with crank angle

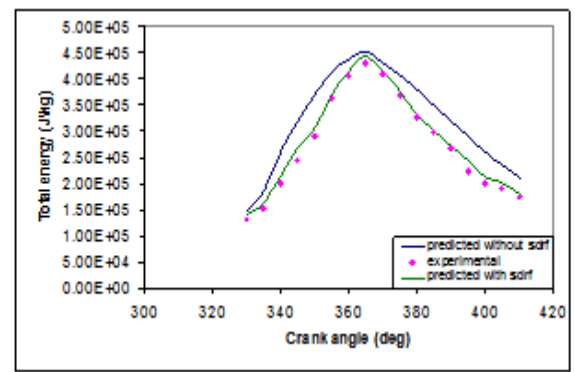
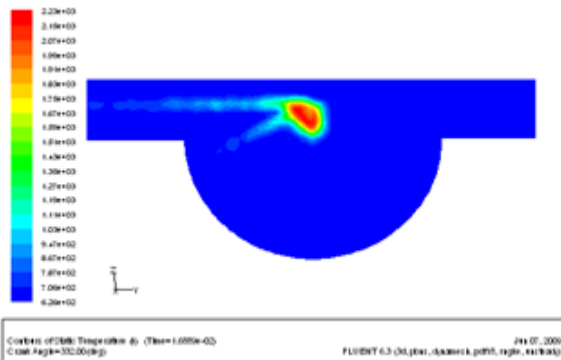
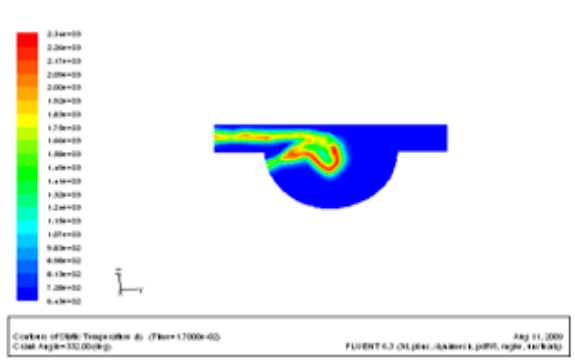


Fig 4.4 variation of total energy with crank angle

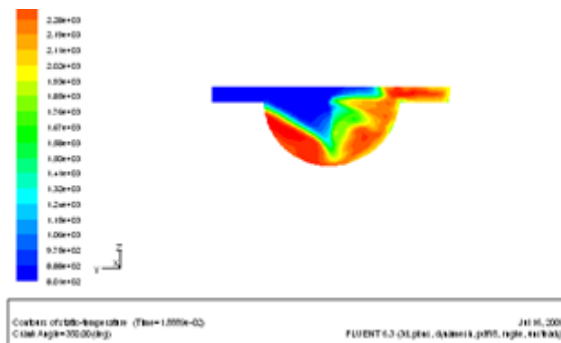


(a₁) At crank angle 28° BTDC without SDRF

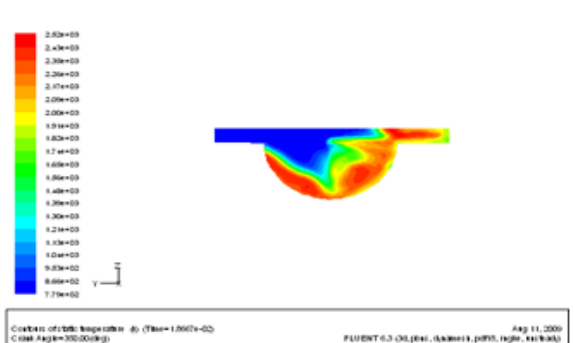


(a₂) At crank angle 28° BTDC with SDRF

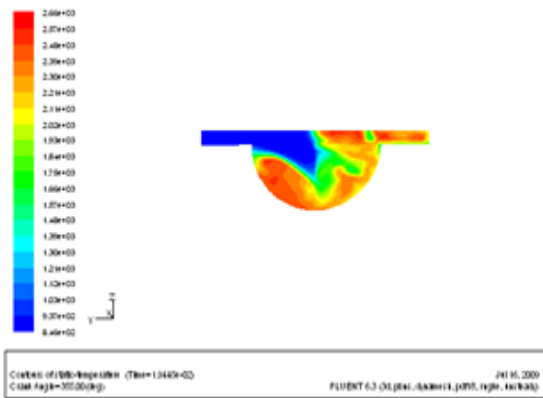
Fig.4.5 Temperature contours at different crank positions



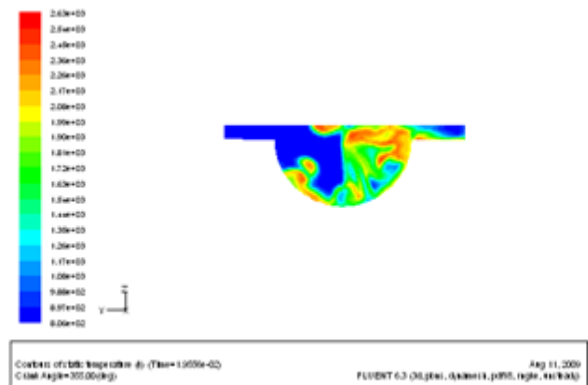
(b₁) At crank angle 10° BTDC without SDRF



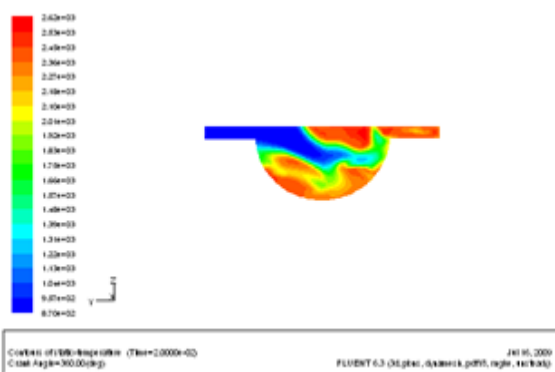
(b₂) At crank angle 10° BTDC with SDRF



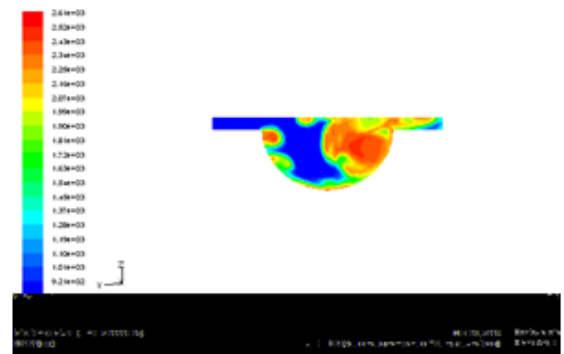
(c₁) At crank angle 5⁰ bTDC without SDRF



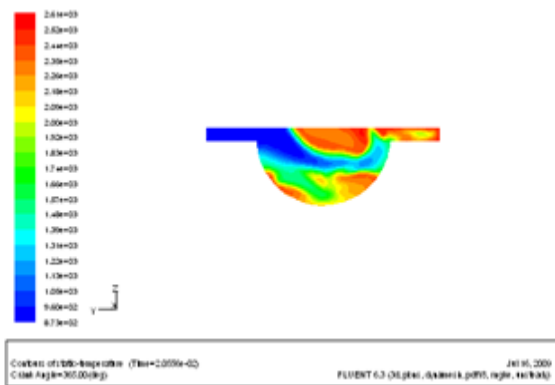
(c₂) At crank angle 5⁰ bTDC with SDRF



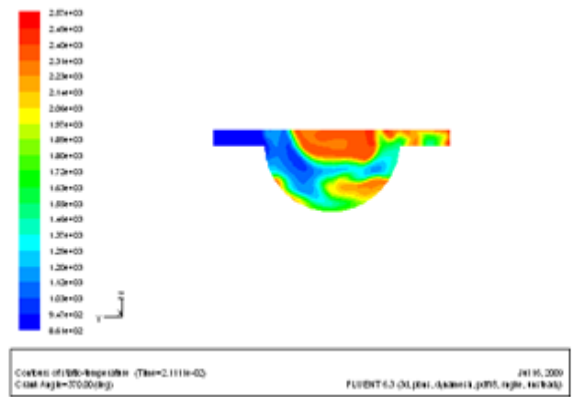
(d₁) At crank angle at TDC without SDRF



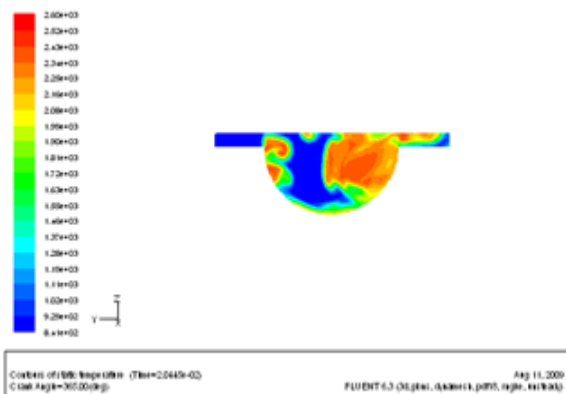
(d₂) At crank angle at TDC with SDRF



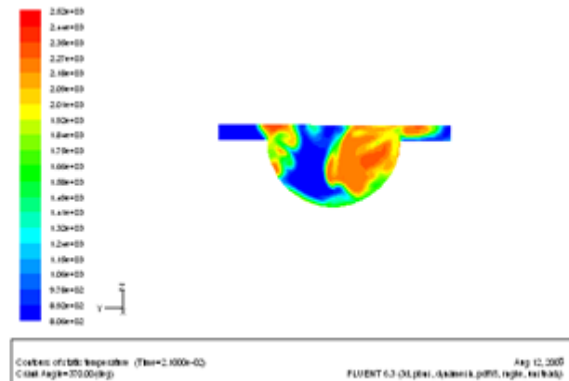
(e₁) At crank angle 5⁰ aTDC without SDRF



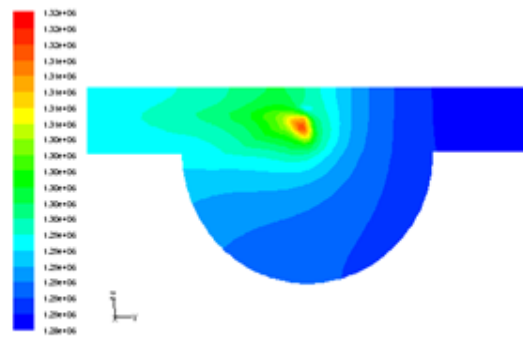
(e₂) At Crank angle 5⁰ aTDC with SDRF



(f₁) At crank angle 10⁰ aTDC without SDRF

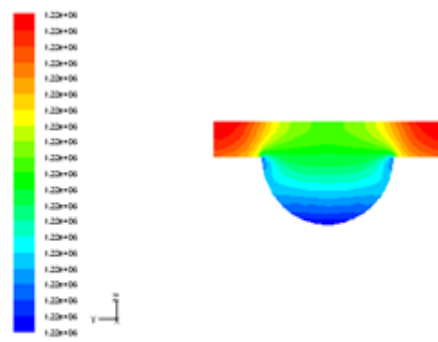


(f₂) At Crank angle 10⁰ aTDC with SDRF



Contours of Static Pressure (contour) (Time=1.0778e-02)
 Crank Angle=352.000(deg) Jan 02, 2009
 FLUENT 6.3 (3d,java, dynamic, pdf, english, windows)

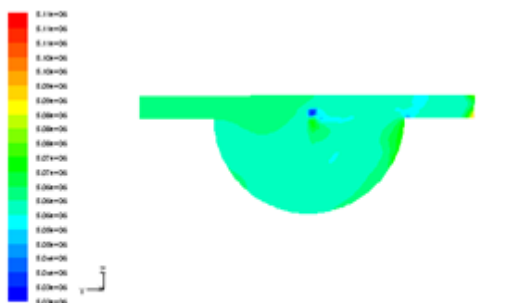
(a₁)At crank angle 28⁰ bTDC without SDRF



Contours of Static Pressure (contour) (Time=1.0778e-02)
 Crank Angle=352.000(deg) Sep 02, 2009
 FLUENT 6.3 (3d,java, dynamic, pdf, english, windows)

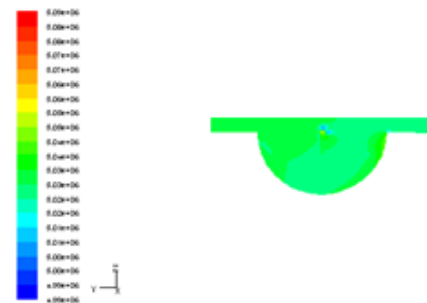
(a₂)At crank angle 28⁰ bTDC with SDRF

Fig.4.6 Pressure contours at different crank positions



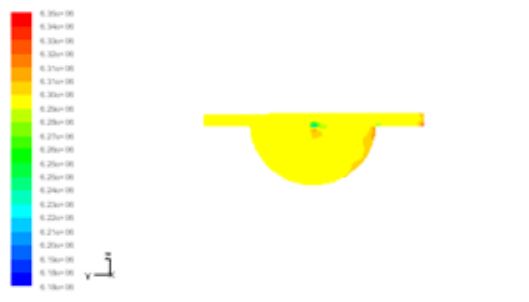
Contours of Static Pressure (contour) (Time=1.0778e-02)
 Crank Angle=352.000(deg) Jan 02, 2009
 FLUENT 6.3 (3d,java, dynamic, pdf, english, windows)

(b₁)At crank angle 10⁰ bTDC without SDRF



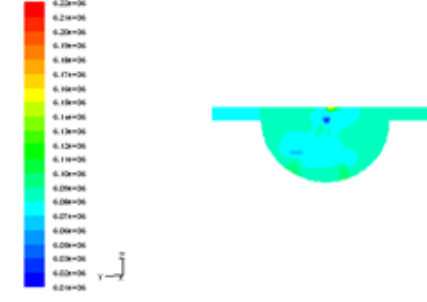
Contours of Static Pressure (contour) (Time=1.0778e-02)
 Crank Angle=352.000(deg) Sep 02, 2009
 FLUENT 6.3 (3d,java, dynamic, pdf, english, windows)

(b₂)At crank angle 10⁰ bTDC with SDRF



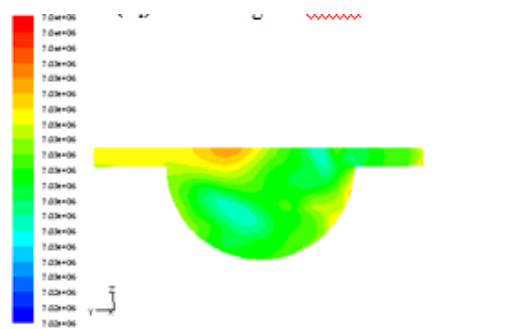
Contours of Static Pressure (contour) (Time=1.0778e-02)
 Crank Angle=352.000(deg) Jan 02, 2009
 FLUENT 6.3 (3d,java, dynamic, pdf, english, windows)

(C₁)At crank angle 5⁰ bTDC without SDRF



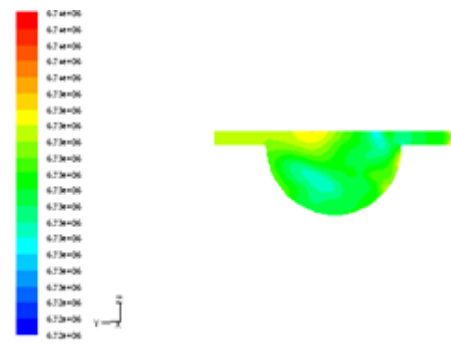
Contours of Static Pressure (contour) (Time=1.0778e-02)
 Crank Angle=352.000(deg) Sep 02, 2009
 FLUENT 6.3 (3d,java, dynamic, pdf, english, windows)

(C₂)At crank angle 5⁰ bTDC with SDRF



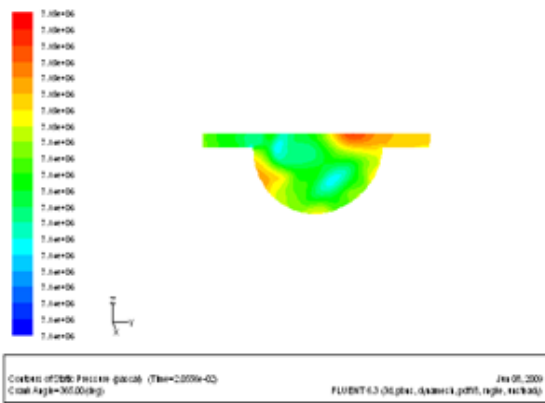
Contours of Static Pressure (contour) (Time=2.0000e-02)
 Crank Angle=360.000(deg) Jan 02, 2009
 FLUENT 6.3 (3d,java, dynamic, pdf, english, windows)

(d₁)At crank angle at TDC without SDRF

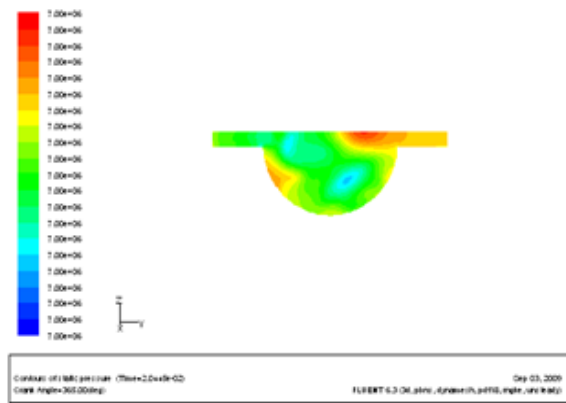


Contours of Static Pressure (contour) (Time=1.0000e-02)
 Crank Angle=360.000(deg) Sep 02, 2009
 FLUENT 6.3 (3d,java, dynamic, pdf, english, windows)

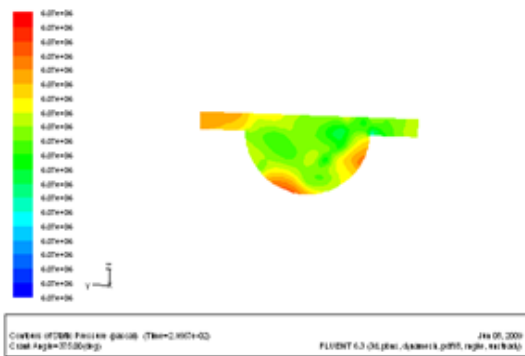
(d₂)At crank angle at TDC with SDRF



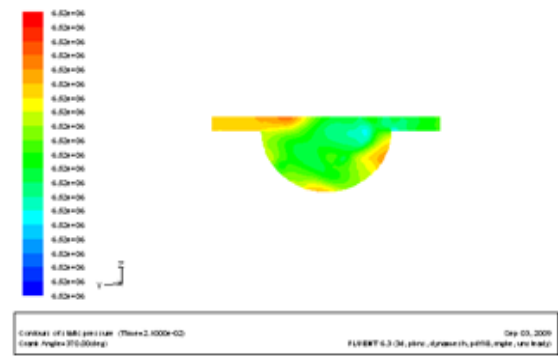
(e₁)At crank angle 5⁰ aTDC without SDRF



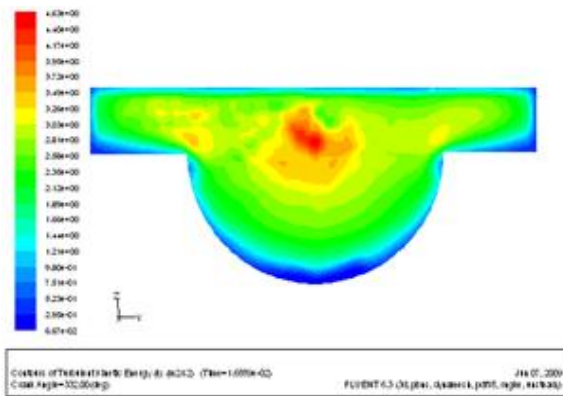
(e₂)At crank angle 5⁰ aTDC with SDRF



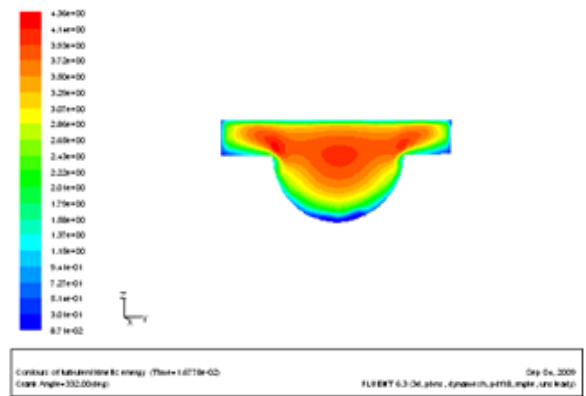
(f₁)At crank angle 10⁰ aTDC without SDRF



(f₂)At crank angle 10⁰ aTDC with SDRF

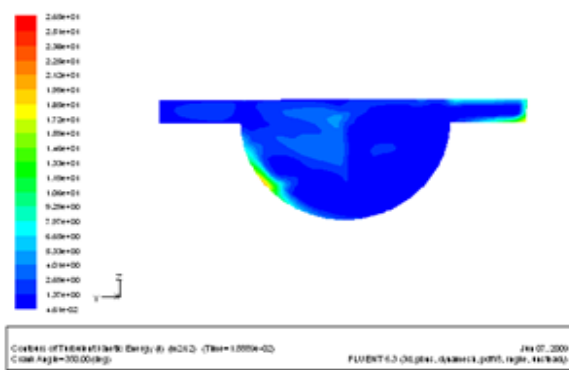


(a₁)At crank angle 28⁰ bTDC without SDRF

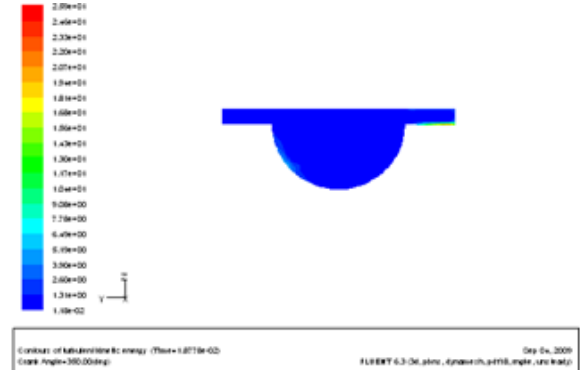


(a₂)At crank angle 28⁰ bTDC with SDRF

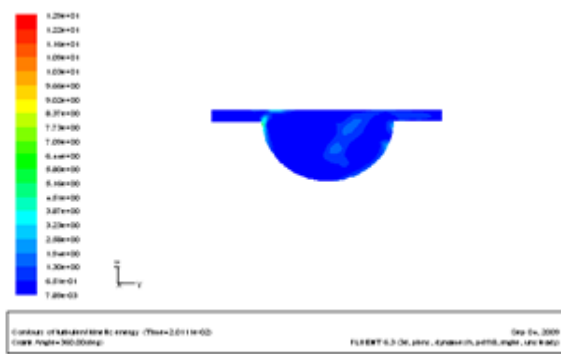
Fig.4.7 Turbulent kinetic energy contours at different crank positions



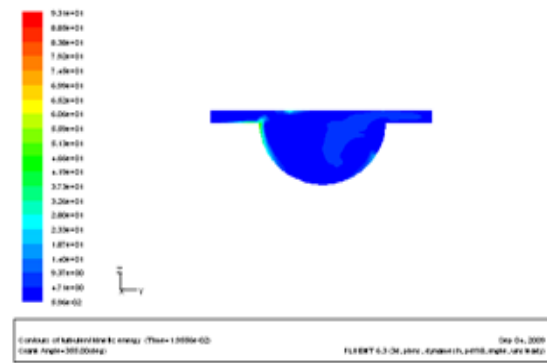
(b₁)At crank angle 10⁰ bTDC without SDRF



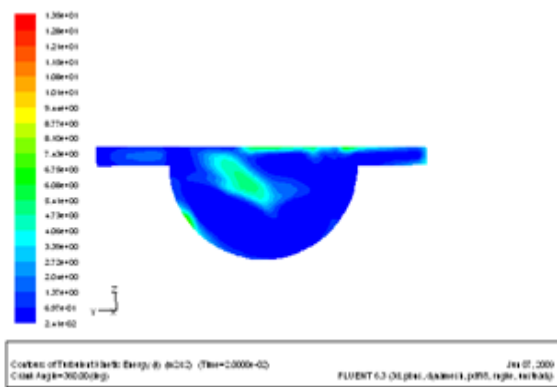
(b₂)At crank angle 28⁰ bTDC with SDRF



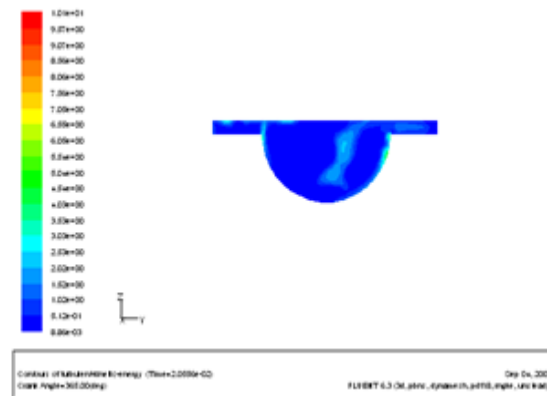
(c₁) At crank angle 5⁰ bTDC without SDRF



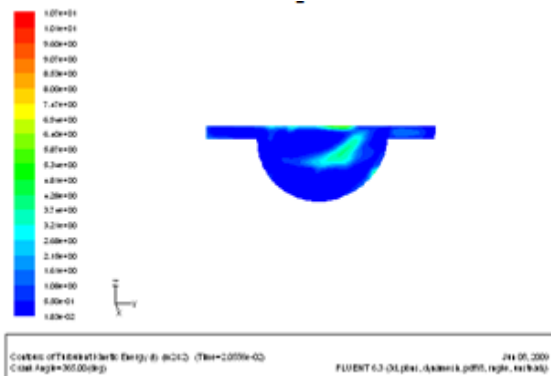
(c₂) At Crank angle 5⁰ bTDC with SDRF



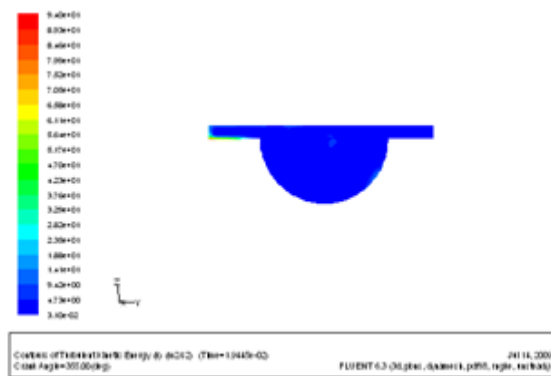
(d₁) Crank angle at TDC with SDRF



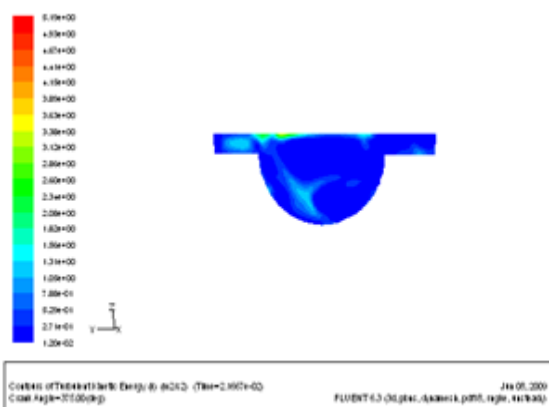
(d₂) Crank angle at TDC with SDRF



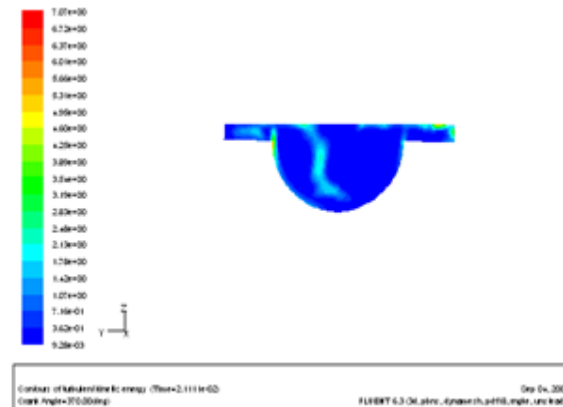
(e₁) At crank angle 5⁰ aTDC without SDRF



(e₂) At crank angle 5⁰ bTDC with SDRF



(f₁) At crank angle 10⁰ aTDC without SDRF



(f₂) At crank angle 5⁰ aTDC with SDRF

V. CONCLUSIONS

SDRF found to have tremendous impact on the in-cylinder flow processes. The predicted results with and without SDRF are compared with the available experimental data. It is concluded that it is better to rely on accounting the effect of SDRF which is nearer to validated results.

The important conclusions from the present paper are presented in the subsequent sections.

5.1 Test Computations:

- The validity of the results accounting SDRF is assessed by comparing the predicted and available measured pressure histories. The results are encouraging as very good agreement is noticed for the pressure histories reducing error percentage between predicted and measured histories and also for temperature variations.
- There is larger deviation in case of total energy for experimental and predicted values and predictions with SDRF come as compromise between the two testifying the importance of inclusion of SDRF.

5.2 Effect of piston bowl configuration:

- At the start of injection, variation in local temperatures can be noticed with SDRF compared to without SDRF. Marginal variation in local temperature is noticed between with and without SDRF when piston is at TDC and when it is moving away from TDC.
- Little variation in local pressure is noticed with and without considering the effect of SDRF. The tip of the injector is spotted to have minimum value of the local pressures in both cases i.e. with and without SDRF.
- Little variation of turbulence level is noticed with and without considering SDRF. Maximum variation in turbulence is noticed at the wall and lip of bowl whereas minimum turbulence is noticed at the bowl region, when piston is towards TDC but when piston is at TDC and away from TDC the turbulence is minimum at the wall and lip region where as it is maximum at bowl region. This argument is valid for both with and without SDRF.

VI. FUTURE SCOPE

There are lot of inconsistencies observed in the predictions and are attributed to the restrictions and assumptions imposed on the codes. Hence the predictive capability of the tool may be increased by possible inclusion of some more restrictions and assumptions

REFERENCES

- [1] K.N.C. Bray and P.A. Libby, The Challenge of Turbulent Combustion, Twenty-Sixth Symposium (International) on Combustion Pages 1-26, The Combustion Institute, Pittsburg, 1996.
- [2] Nobert Peters, Turbulent Combustion, Cambridge university Press, 2000.
- [3] P.A. Libby and F.A. Williams, Fundamental Aspects and a Review in Turbulent Reacting Flows, pages 1-61 Academic Press, London, 1994.
- [4] S.B. Pope, PDF Methods for Turbulent reactive flows, Energy Combst. Sci. Vol. 11, pp 119-192, 1985.
- [5] "FLUENT User Manual", FLUENT 6.3 Documentation, FLUENT International Corporation Ltd.
- [6] K. Rajagopal, Three dimensional Modeling of In-Cylinder Flows, Fuel-Air Mixing and Combustion in a Four Stroke Compression Ignition Engine, Ph.D Theses, IIT Madras, March 1991.
- [7] A.Linan and F.A Williams, Fundamental aspects of combustion, Oxford University Press. New York. 1993.
- [8] S.K. Liew, K.N.C.Bray and J.B. Moss, A Stretched Laminar Flamelet Model of Turbulent Non Premixed Combustion. Combustion Flame 56, 199-213, 1984.

ABOUT THE AUTHOR



journals. Member of MISTE

Dr. S M Jameel Basha is currently working as professor and principal, VIF college of engineering and Technology, Hyderabad. Research interests are IC engines and Heat transfer. Has 16 years of academic and research experience and presented several research papers in various international and national professional bodies as MIE,